# Polymer-Coated Nanoparticles Interacting with Proteins and Cells: Focusing on the Sign of the Net Charge

**Dominik Hühn,[†,⊗] Karsten Kantner,[†,⊗] Christian Geidel,[‡] Stefan Brandholt,[§] Ine De Cock,[⊥] Stefaan J. H. Soenen,[⊥] Pilar Rivera_Gil,[†] Jose-Maria Montenegro,[†] Kevin Braeckmans,[⊥] Klaus Müllen,[‡] G. Ulrich Nienhaus,[§,∥,#] Markus Klapper,[‡,*] and Wolfgang J. Parak[†,▽,*]**

[†]Department of Physics, Philipps-University Marburg, Marburg, Germany, [‡]Max Planck Institute for Polymer Research, Mainz, Germany, [§]Institute of Applied Physics and Center for Functional Nanostructures (CFN), Karlsruhe Institute of Technology (KIT), Karlsruhe, Germany, [⊥]Faculty of Pharmaceutical Sciences, Ghent University, Ghent, Belgium, [∥]Institute of Toxicology and Genetics, Karlsruhe Institute of Technology (KIT), Karlsruhe, Germany, [#]Department of Physics, University of Illinois at Urbana-Champaign, Urbana, Illinois 61801, United States, and [▽]CIC biomaGUNE, San Sebastián, Spain. [⊗]Both authors contributed equally to this work.

**ABSTRACT** To study charge-dependent interactions of nanoparticles (NPs) with biological media and NP uptake by cells, colloidal gold nanoparticles were modified with amphiphilic polymers to obtain NPs with identical physical properties except for the sign of the charge (negative/positive). This strategy enabled us to solely assess the influence of charge on the interactions of the NPs with proteins and cells, without interference by other effects such as different size and colloidal stability. Our study shows that the number of adsorbed human serum albumin molecules per NP was not influenced by their surface charge. Positively charged NPs were incorporated by cells to a larger extent than negatively charged ones, both in serum-free and serum-containing media. Consequently, with and without protein corona (*i.e.*, in serum-free medium) present, NP internalization depends on the sign of charge. The uptake rate of NPs by cells was higher for positively than for negatively charged NPs. Furthermore, cytotoxicity assays revealed a higher cytotoxicity for positively charged NPs, associated with their enhanced uptake.

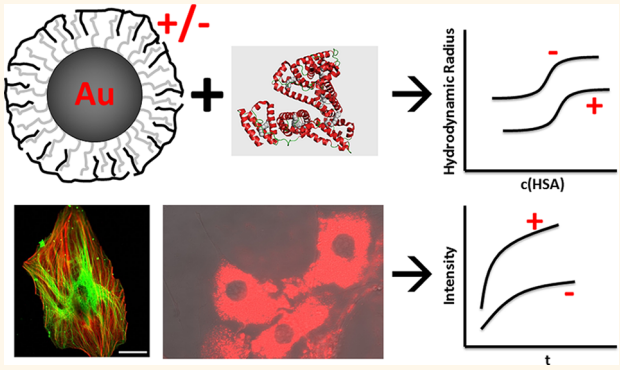


**KEYWORDS:** colloidal gold nanoparticles · surface charge dependence · protein corona · uptake by cells · cytotoxicity

Although cytotoxicity of colloidal nanoparticles (NPs) is currently under intensive research, we are not yet at the point where we understand how cytotoxic effects are related to key physicochemical parameters of the NPs such as colloidal stability, size, surface charge, *etc.*[1,2] This is partly due to the fact that some of these properties are hard to control and study individually. In fact, it is challenging to prepare a set of NPs for which only a single property is varied because they are often interrelated.[1]

Charge is a key parameter of NPs known to influence their cellular uptake as well as cytotoxicity.[3−11] In studies of charge-dependence, negative or positive net surface charge is often introduced *via* surfactants bearing $-COO^-$ or $-NH_3^+$ groups, respectively. However, the protonation state of these groups and, therefore, the net charge depend on the surrounding pH. Moreover, changes in net charge can drastically affect colloidal stability. pH is a very important factor because it changes along the internalization pathway from slightly alkaline in the cell medium (7.4−7.0) to highly acidic in intracellular vesicles (5.0−4.6).[12] Limitations in colloidal stability can be partly avoided by using proteins or polyethylene glycol (PEG) terminated with $-COO^-$ or $-NH_3^+$ groups as ligands.[13,14,15] In this work, we introduce charge by enshrouding the NP with an amphiphilic diblock-copolymer containing blocks of monomers with a long, hydrophobic alkyl side chain and blocks of monomers that carry charge (Figure 1). Phosphonate ($-PO(OH)_2$) and trimethylammonium ($-N(CH_3)_3$) groups provide a permanent negative and positive charge,

* Address correspondence to wolfgang.parak@physik.uni-marburg.de, klapper@mpip-mainz.mpg.de.

Received for review December 21, 2012 and accepted March 26, 2013.

**Published online March 26, 2013**
**10.1021/nn3059295**

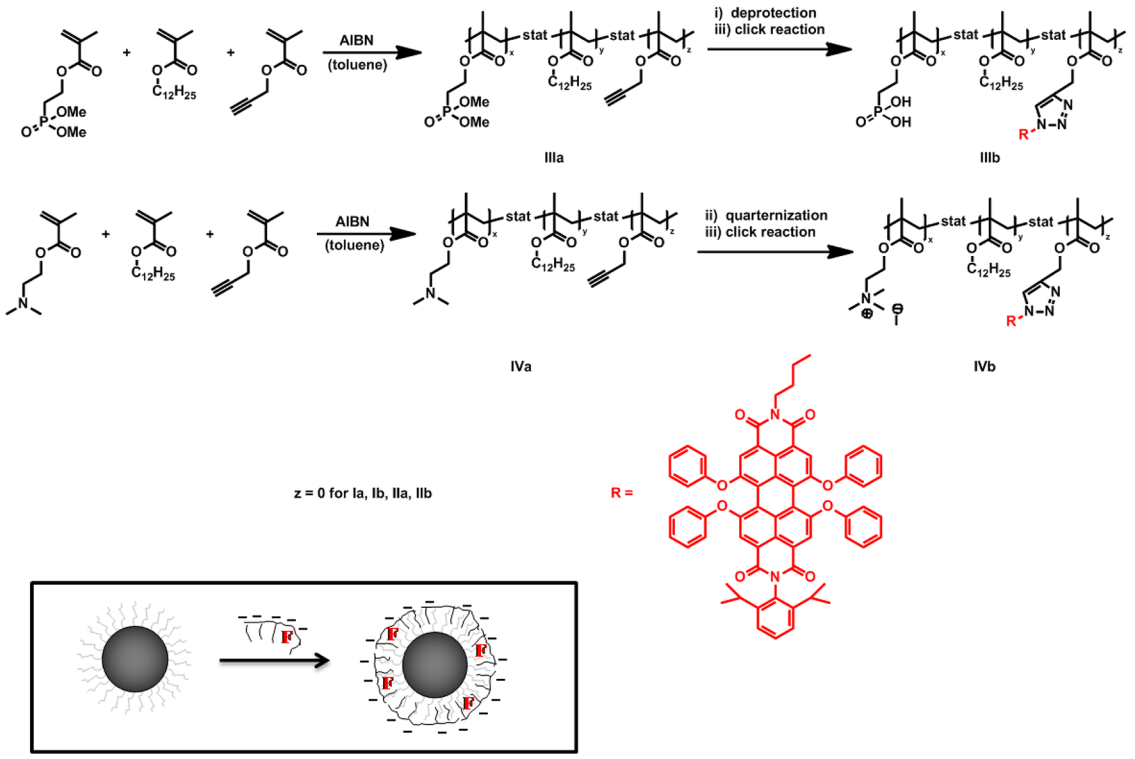


**Figure 1. Copolymers and fluorophore-functionalized terpolymers for coating the hydrophobic Au NPs. A detailed description is given in the Supporting Information. (i) Deprotection with trimethylsilyl bromide in dichloromethane; (ii) quaternization of the amino function with methyliodide in dichloromethane; (iii) click reaction with dye-azide (PDI-$N_3$), CuI, and *N*,*N*,*N*′,*N*′,*N*″-pentamethyldiethylenetriamine in toluene. IIIa and IVa refer to the negatively and positively charged terpolymers with an alkyne residue. IIIb and IVb refer to the negatively and positively charged fluorescent terpolymers. For the nonfluorescent copolymers (Ia/Ib = negatively charged; IIa/IIb = positively charged), the alkyne comprising monomer has to be neglected in each case ($z = 0$). Box: Scheme of the polymer coating procedure. Au NPs were capped with hydrophobic surfactants (dodecanethiol). An amphiphilic polymer with monomers comprising hydrophobic side-chains, monomers comprising polar groups, and optionally monomers comprising a fluorophore (F) can be wrapped around the NP driven by hydrophobic interaction. Upon exposure of the polar groups on the surface, the NPs can be suspended in water. Negatively or positively charged NPs are obtained, depending on the polar group of the polymer.**

respectively. The first $pK_a$ value of the $-PO(OH)_2$ ($pK_{a1} = 2.4$) is low enough to provide a negative charge under all pH conditions that NPs may experience outside and inside cells, *cf.* Figure 1.[16] For negatively as well as for positively charged NPs, the charged groups are situated at the same polymer backbone, so that the surface properties of the NPs are—to a very good approximation—identical except for the sign of the charge. The polymer is wrapped around the surface of dodecanethiol-capped Au NPs.[16] The hydrophobic side chains of the polymer intercalate with the hydrophobic dodecyl chains on the Au cores, and the charged blocks point toward the surrounding solution so as to provide excellent colloidal stability in an aqueous environment (Figure 1). The resulting NPs are very well-defined and enable a detailed analysis of their physicochemical parameters.

We hypothesized that the different charge on the NPs may affect cellular uptake and their subsequent cytotoxicity along two different routes. On the one hand, charge could directly influence the interaction with cells. On the other hand, charge could change the protein corona around the NP surface, which would indirectly modify cell-NP interactions. To resolve these issues, we have investigated both, the charge dependence of the protein corona as well as the charge dependence on NPs uptake under serum-containing (*i.e.*, in the presence of a protein corona) and under serum-free conditions (*i.e.*, in the absence of a protein corona). In addition, the charge-dependence of the cytotoxicity was studied using a variety of methods. Notably, due to the high colloidal stability of the NPs, the effects of charge could be examined without interference by changes in NP size or colloidal stability.

## RESULTS AND DISCUSSION

**Physicochemical Characterization.** The charge on the as-synthesized NPs was determined by $\zeta$-potential measurements on NPs without fluorophores in in Milli-Q water (medium #1) to be $-39.8 \pm 10.0$ mV and $+9.7 \pm 8.9$ mV for the negatively and positively charged NPs (*cf.* Table 1 and Figure 1 about their surface chemistry), respectively. Hydrodynamic diameters of NPs were recorded in phosphate-buffered saline (PBS) (medium #2) with dynamic light scattering (DLS, as determined from the number distribution) and with fluorescence

**TABLE 1. Composition of the Amphiphilic Co- and Terpolymers**

| | composition of the polymer[a] | | | | | |
|---|---|---|---|---|---|---|
| polymer | TMAEMA [mol %] | MAPHOS [mol %] | LMA [mol %] | PgMA [mol %] | $M_n$[b] [g mol$^{-1}$] | PDI[c] |
| **Ib** | - | 40 | 60 | - | 9000 | 2.0 |
| **IIb** | 53 | - | 47 | - | 16300 | 1.8 |
| **IIIb** | - | 52 | 42 | 6 | 9500 | 2.1 |
| **IVb** | 48 | - | 48 | 4 | 17800 | 2.0 |

[a] Determined *via* $^1$H NMR-spectroscopy. [b] Molecular weights were determined by GPC in THF *versus* PMMA standard after the initial reaction step (polymerization of the protected/neutral monomers; **Ia** – **IVa**). The presented $M_n$ values were recalculated for the final polymers (**Ib** – **IVb**). [c] PDI: polydispersity index.

correlation spectroscopy (FCS). While a fluorescent polymer shell was required for FCS, fluorescence would have interfered with DLS. Thus, DLS measurements were performed with NPs without fluorophores in the polymer shell. Hydrodynamic diameters, $d_h$, of negatively and positively charged NPs were determined as 14.5 ± 1.0 nm (DLS) and 15.8 ± 0.4 nm (FCS), and 10.1 ± 0.6 nm (DLS) and 10.2 ± 0.2 nm (FCS), respectively, *cf.* Table 2. Within the experimental errors, DLS and FCS yielded comparable results, however, FCS results had smaller errors and, in our hands, were better reproducible. The negatively charged NPs are slightly bigger than the positively charged ones. This might be due to a charge effect, so that a higher ζ-potential results in a further extended Stern double layer. Consequently, the hydrodynamic diameter correlates with the magnitude of the ζ-potential.[17] As the magnitude of the ζ-potential of negatively charged NPs was approximately four times higher than that of the positively charged NPs, the difference in hydrodynamic diameter is consistent with this interpretation.

It is well-known that counterions can screen the charge of the NPs and, thereby, cause instability of colloidal properties.[18,19] To examine this effect, colloidal stability was probed using 5 nM NP suspensions in the following solutions which are relevant as cell culture media (water as Medium #1 was used as reference): Medium #2, PBS; Medium #3, Dulbecco's modified Eagle's medium (DMEM); Medium #4, PBS + 1% penicillin/streptomycin (P/S) + 1% L-glutamine (L-Glu); Medium #5, DMEM + 1% P/S + 1% L-Glu; Medium #6, PBS + 800 μM bovine serum albumin (BSA); Medium #7, DMEM + 1% P/S + 1% L-Glu + 800 μM BSA; Medium #8, DMEM + 1% P/S + 1% L-Glu + 10% fetal bovine serum (FBS). Colloidal stability was first probed *via* UV/vis spectroscopy by recording changes in the normalized absorbance (*cf.* Figures 2a,b) at the surface plasmon resonance (SPR) of Au NPs. The idea was to attribute changes in absorbance to reduced colloidal stability. Typically, when Au NPs agglomerate, their plasmon peak broadens and shifts to the red,

**TABLE 2. Results of the FCS Data[a]**

| NP charge | $r_h(0)$ [nm] | $r_h(N_{max})$ [nm] | $\Delta r_h$ [nm] | $N_{max}$ | $K_d$ [μM] | $n$ |
|---|---|---|---|---|---|---|
| negative | 7.9 ± 0.2 | 10.4 ± 0.3 | 2.5 ± 0.2 | 32 ± 4 | 1.5 ± 0.8 | 0.8 ± 0.3 |
| positive | 5.1 ± 0.1 | 9.4 ± 0.4 | 4.3 ± 0.4 | 35 ± 3 | 1.0 ± 0.3 | 0.8 ± 0.3 |

[a] $r_h(0)$ is the hydrodynamic radius of bare NPs without protein corona (as determined at a HSA concentration of $1 \times 10^{-4}$ μM and $2 \times 10^{-5}$ μM for negatively and positively charged NPs, respectively), $r_h(N_{max})$ is the hydrodynamic radius of the NPs saturated with HSA, $\Delta r_h = r_h(N_{max}) - r_h(0)$ the thickness of the protein corona, $N_{max}$ is the maximum number of adsorbed HSA molecules per NP, $K_d$ is the apparent binding constant, and $n$ *is* the Hill coefficient. We noted that the positively charged NPs started to agglomerate at HSA concentrations above 3 μM, as inferred from the increasing molecular brightness (see Supporting Information).

which would give rise to a reduced absorbance at the wavelength of the original plasmon peak.[20] For the incubation experiments in Figure 2, DMEM without the pH indicator phenol red was used. In case phenol red is present in DMEM (media #3, #5, #7), the absorption of the dye itself changes over time and thus may lead to misinterpretation, *cf.* the Supporting Information. As second indicator for colloidal stability, changes in the hydrodynamic diameter $d_h$ upon incubation in the different media were recorded with DLS (*cf.* Figure 2c,d). However, these measurements were possible only in the media without proteins (media #2, #3, #4, #5), as proteins themselves contributed to light scattering and thus interfered with determination of $d_h$, *cf.* the Supporting Information. The results obtained with UV/vis spectroscopy (*cf.* Figures 2a,b) indicate that incubation in media without BSA (media #2, #3, #4, #5, #8) did not lead to changes in the absorption profile. Especially noteworthy is the colloidal stability of Au NPs in medium #8, the most relevant one for cell culture and uptake experiments. Presence of BSA as the only protein (media #6, #7), however, led to changes (increase of the relative absorbance) at the surface plasmon peak over time for negatively and positively charged NPs, although the plasmon peak was still resolved without significant broadening. Thus, these changes may not result from the formation of (large) agglomerates, but from adsorption of BSA proteins, which changes the absorbance behavior while maintaining colloidal stability. However, this effect was the same for both polarities, and therefore, the effect on the NPs of opposite charge on cells is comparable. DLS data (Figure 2c,d) indicate a different situation. No change in $d_h$ over time was found for positively charged NPs in all media without protein component (media #2, #3, #4, #5), whereas $d_h$ was constant over time only for negatively charged NPs immersed in medium #2. In the other media (#3, #4, #5), agglomeration of negatively charged Au NPs was observed directly after addition of the medium. Interestingly, even the small content of P/S and L-Glu, whether in PBS (medium #4) or in DMEM (medium #5), had a pronounced and reproducible effect. These data

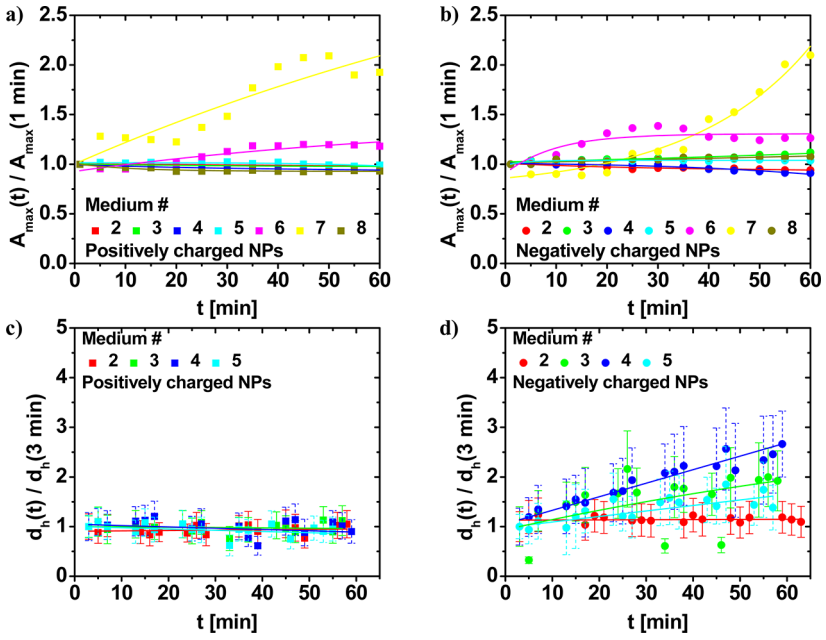


**Figure 2. Stability tests in different media (#2, PBS; #3, DMEM; #4, PBS + 1% P/S + 1% L-Glu; #5, DMEM + 1% P/S + 1% L-Glu; #6, PBS + 800 $\mu$M BSA; #7, DMEM + 1% P/S + 1% L-Glu + 800 $\mu$M BSA; #8, DMEM + 1% P/S + 1% L-Glu + 10% FBS). (a and b) The time dependent evolution of the absorbance $A_{max}(t)$ at the surface plasmon peak normalized to absorbance at the surface plasmon peak after 1 min of incubation, $A_{max}$(1 min), for positively and negatively charged Au NPs without fluorophore in the shell. The spectra and a UV/vis series including DMEM with pH indicator for Au NPs with and without fluorophore in the shell are shown in the Supporting Information. The pure medium always served as blank. (c and d) The time dependent evolution of the hydrodynamic diameter $d_h(t)$ normalized to the hydrodynamic diameter after 3 min of incubation, $d_h$(3 min), for positively and negatively charged Au NPs without fluorophore in the shell as recorded by DLS. The absolute hydrodynamic diameters are provided in the Supporting Information. For a–d, the type of the medium is indicated in color, the charge of the NPs by the symbol (square, positively charged NPs; circle, negatively charged NPs). The lines are drawn to guide the eye.**

suggest that our negatively charged NPs are colloidally less stable than the positively charged ones. This is further supported by the optical microscopy data (*cf.* Figure 4), which qualitatively suggest the presence of more agglomerates for negatively charged NPs. We note, however, that FCS data showed more agglomerates for positively charged NPs at high protein concentrations (*cf.* the Supporting Information).

In summary, our data indicate that colloidal stability in complex media cannot be trivially assessed, and different methods show different sensitivity. Changes in the UV/vis spectra are less sensitive to the formation of small agglomerates than changes in the hydrodynamic diameter as detected by DLS. However, as the size of the present NPs is at the lower detection limit of the used DLS instrument, those results also have to be interpreted with care. We conclude that the negatively charged NPs used in this study show the tendency to form (small) agglomerates in the media used for cell culture. Bigger agglomerates would have been visible in the UV/vis spectra and thus are not predominantly formed. No effect on the different media on their colloidal stability has been observed for the positively charged NPs. Thus, differences in colloidal stability between the negatively and the positively charged NPs upon their interaction with cells need to be considered.

**Investigation of Protein Adsorption.** NPs in biological media are coated by a so-called protein corona,[21,22] which may influence both the colloidal stability of NPs and NP uptake by cells.[23] To probe the charge dependence of the protein corona, we used serum albumin as a model protein (bovine: BSA, human: HSA) with a similar concentration as the FBS proportion of medium #8. Because serum albumin is the most abundant protein in blood serum, a detailed study was performed with this protein using FCS. Because of compatibility reasons with previous studies, HSA was used instead of BSA.[24] The hydrodynamic radius of the Au NPs increased with increasing HSA concentration due to adsorption of HSA, and saturated for HSA concentrations around 10 $\mu$M, *cf.* Figure 3. Fitting of the results with the Hill model yielded the hydrodynamic radii of the NPs without and with saturated protein corona, the maximum number of adsorbed HSA molecules per NP, the apparent binding constant, and the Hill coefficient, *cf.* Table 2.

In summary, the adsorption of HSA showed the same qualitative behavior on the negatively and positively charged NPs. For both, the best fit yields a slightly anti-cooperative behavior, the adsorbed proteins form a monolayer on the NP surface, and a similar number of HSA molecules is adsorbed per NP.[25] Compared to the results with FePt NPs coated with a similar negatively charged reference polymer,[24] the binding affinity is

decreased by a factor three for the negatively and by a factor five for the positively charged NPs. For the negatively charged NPs, this discrepancy may result from the fact that the negatively charged polymer used in this study had a lower charge density than the negatively charged reference polymer.[16] However, our data are not sensitive to the conformation of the adsorbed HSA molecules, which may differ in both cases. We note that our protein adsorption study utilizes a single, well-defined model protein, HSA. However, serum contains a huge number of proteins which all may be involved in protein corona formation.[26] It was shown that HSA may be displaced from the NP surface by other proteins,[27] which resulted in differences in the protein corona around negatively and positively charged NPs.[11,22] Furthermore, the amount of adsorbed proteins per NP also depends on their type and conformational properties.[28] Taken together, although we are not sensitive to conformational changes of the adsorbed HSA on negatively and positively charged NPs, our data clearly reveal that the amount of adsorbed HSA on our NPs is not strongly affected by the sign of the charge.

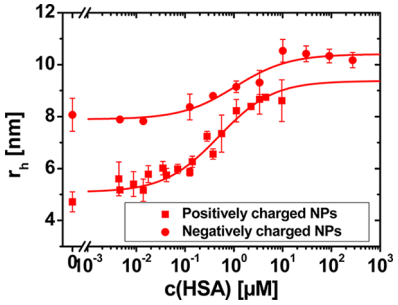


**Figure 3. HSA concentration dependent increase of the hydrodynamic radius $r_h$ of positively and negatively charged Au NPs as recorded in PBS (medium #2). Each data point represents an average from three independent measurements.**

**Charge-Dependent Uptake of Nanoparticles.** 3T3 fibroblast cells were incubated in different media with negatively and positively charged NPs with red fluorophores in the shell. As cell media, we selected buffers without proteins (medium #5) and buffers supplemented with 800 $\mu$M BSA (medium #7) or with 10% FBS (medium #8), to take into account effects of the protein corona. NPs were incorporated by cells, as concluded by the accumulation of red fluorescence inside the cells (*cf.* Figure 4). Granular distribution suggests the presence of the NPs in intracellular vesicles such as endosomes and lysosomes, in accordance with the literature.[8,29−33] Fluorescence originating from internalized NPs was quantified from microscopy images (transmission and red fluorescence channel) and is plotted in Figure 4 as fluorescence intensity *versus* time. The intensities were corrected for background and intrinsic differences of the fluorescence behavior

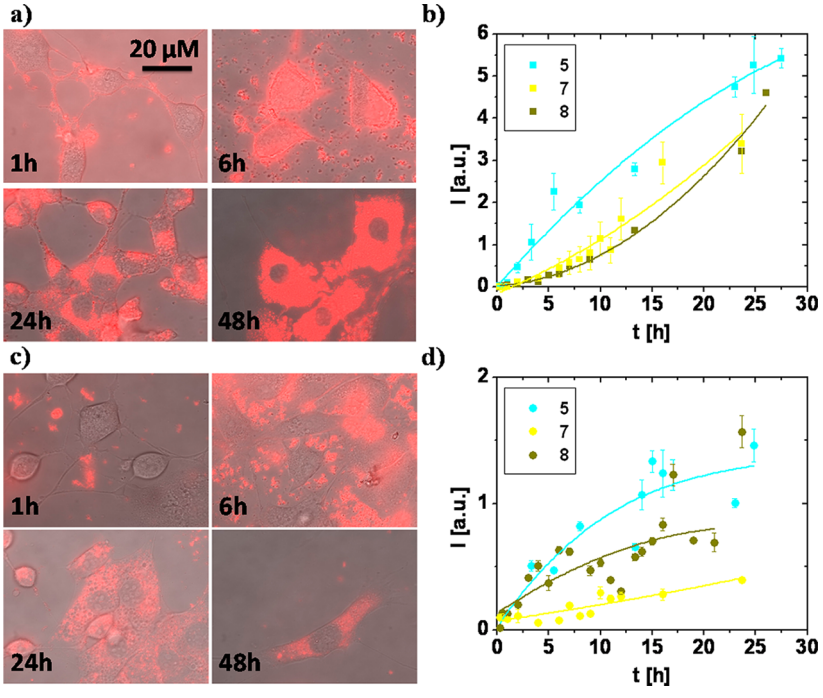


**Figure 4. 3T3 fibroblasts were incubated with (a) positively and (c) negatively charged Au NPs in different culture media. The images show the cells at different times (as indicated in each panel) after incubation in medium #8 (dark field overlaid with fluorescence channel). Brightness differs slightly due to environmental influences (day light); the data were background-corrected for further analysis (see Supporting Information). The average fluorescence intensity ($I$) per cell (background corrected) for (b) positively and (d) negatively charged NPs is plotted *versus* incubation time for media #5, #7 and #8. The uptake rate of positively charged Au NPs was significantly higher compared to negatively charged Au NPs. The scale of the fluorescence intensity axes is arbitrary but chosen so as to enable a quantitative comparison. Lines are drawn to guide the eye.**

of negatively and positively charged NPs (a detailed description of the data correction is part of the Supporting Information). A significant difference between the uptake rates of negatively and positively charged NPs was observed; uptake of positively charged NPs was significantly faster (*cf.* the slope of fluorescence intensity). Already 1 h after incubation, attachment of positively charged NPs to the outer cell membrane (which is overall negatively charged) can be observed. This difference is likely explained by electrostatic attraction of the positively charged NPs toward the negatively charged cell membrane.[34−36] After two days, significantly more positively charged NPs were internalized per cell than negatively charged NPs (absolute fluorescence intensity). Our data analysis hereby allowed for distinction between adherent and incorporated NPs (*cf.* Supporting Information). Differences in uptake are in agreement with other studies in which enhanced uptake of positively charged NPs has been reported.[37−40] Our data also allow for analyzing the dependence of uptake from the presence of the protein corona. As has been demonstrated above, both negatively and positively charged NPs in media #7 and #8 are assumed to be saturated with proteins on their surface (*cf.* also Figure 3), whereas no proteins are present in medium #5. As can be seen from Figure 4, the presence of proteins slows the uptake of NPs independent of their charge.[41,42] This behavior is in accordance with other studies, however, the extent of that difference is not as pronounced in our study.[43]

The observed differences in uptake yield clearly depend on the employed cell media.[23] However, because both, negatively and positively charged NPs have been incubated with the same media, the charge dependence of the uptake in the different media can be analyzed. To further investigate the differences in uptake levels of the negatively and positively charged NPs in relation to differences in medium composition and cell type, the NPs were used to label murine C17.2 neural progenitor cells (NPCs) and human umbilical vein endothelial cells (HUVECs). Afterward, their fluorescence intensities were recorded by flow cytometry (*cf.* Figure 5a,b). Standard fluorescence measurements by using FACS cannot distinguish well between internalized NPs and NPs adhering to the outer cell membrane,[44] despite washing. Thus, the FACS data quantify the overall amount of cell-associated NPs. The data clearly show higher levels of cell-associated positively charged NPs for both cell types, at both 2 and 24 h of incubation (*cf.* Figure 5a,b). This is in accordance with data obtained using the microscopy analysis in this study for 3T3 fibroblasts and with literature data.[45] Furthermore, uptake levels of negatively charged NPs were similar for the two cell types, whereas positively charged NPs were associated much more with the NPC than with the HUVECs, demonstrating clear cell type-dependent uptake characteristics that are most pronounced for the positively charged NPs. The latter may reflect differences in the media composition used for the two cell types, where the positively charged NPs may form agglomerates in the serum-rich media used for the NPCs, whereas the NPs are more stable in the serum-low media used for the HUVECs. Alternatively, differences in the plasma membrane composition of the cell types and intrinsic differences in the cellular endocytosis levels and mechanisms of either cell type may further contribute to these differences.

In summary, cellular uptake experiments clearly demonstrate enhanced internalization of positively charged NPs compared to negatively charged ones. Presence of proteins in the media reduces NP uptake regardless of the charge of the NPs.

**Charge-Dependent Cytotoxicity of Nanoparticles.** Mechanistic explanations of enhanced toxicity by positively charged NPs are still under discussion.[46] For this reason, we directly compared NPs with negative and positive net charge that were otherwise essentially identical. HUVECs and C17.2 cells were exposed to various concentrations of the Au NPs to examine differences in cytotoxic effects of the NPs related to their surface charge. Multiple parameters typically associated with the cytotoxic profile of engineered NPs were tested, including cell viability, induction of oxidative stress, cell morphology and stem cell functionality.[6,47] The data show a clear concentration-dependent decrease in cell viability for the positively charged NPs, whereas no effects were observed for the negatively charged NPs up to a concentration of 50 nM (*cf.* Figure 5c). Interestingly, the observed decrease in cell viability for positively charged NPs correlated well with increased oxidative stress in both cell types (*cf.* Figure 5d), suggesting an important role of oxidative stress in the cytotoxic effects of the positively charged NPs, which is in line with available literature data.[48,49] To further evaluate possible effects of the NPs on cell homeostasis, alterations in the morphology of HUVECs cells at non-cytotoxic NP concentrations were assessed. The results show, that despite the absence of cytotoxic effects, both types of NPs display concentration-dependent decreases in cell spreading and effects on the actin cytoskeleton (*cf.* Figure 5e). Such effects of Au NPs on cellular cytoskeleton architecture have been described in a few reports.[50,51] We also evaluated the differentiation potential of C17.2 NPC cells upon exposure to Au NPs at non-cytotoxic concentrations. Figure 5f shows a clear diminution of cell differentiation for cells exposed to the positively charged Au NPs at 5 nM or above, in contrast to the negatively charged NPs, which did not induce any effects at concentrations up to at least 20 nM.

Upon internalization, NPs subsequently translocate to different cellular compartments until they reach their final destination.[52] Thus, cytotoxic effects also need to be seen in the context of the intracellular

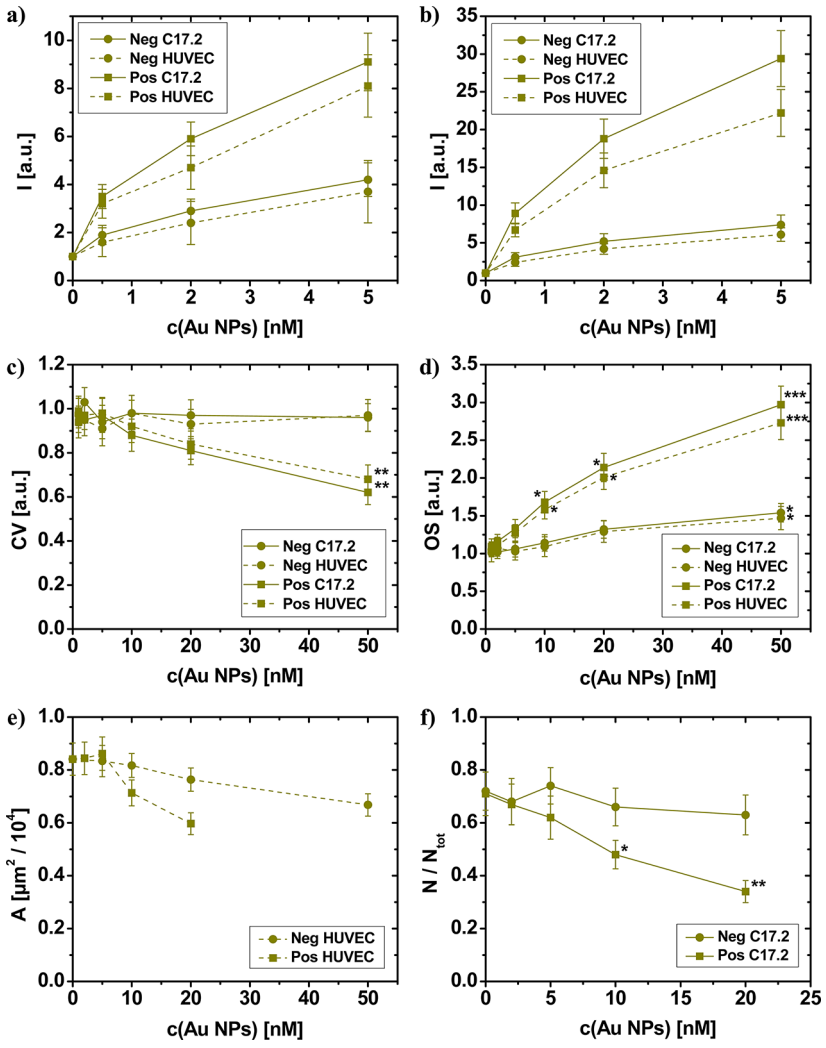


**Figure 5. Fluorescence-activated cell sorting (FACS) results (*I* = fluorescence intensity) for (a) 2 h and (b) 24 h of incubation in medium similar to medium #8 (*cf.* Supporting Information). Data are normalized to *I* at *c*(Au NPs) = 0 nM. (c) Cell viability (CV) for C17.2 neural progenitor cells and primary HUVEC cells as assessed by an Alamar blue assay after 24 h incubation. Data are expressed relative to untreated control cells as mean ± standard deviation (SD; *n* = 4). A value of 1.0 corresponds to 100%. (d) Levels of oxidative stress (OS) for C17.2 neural progenitor cells and primary HUVEC cells as assessed by $H_2$DCFDA after 24 h incubation. Data are expressed relative to untreated control cells as mean ± SD (*n* = 3). A value of 1.0 corresponds to 100%. (e) The average cell areas (*A*) of HUVEC cells after 24 h incubation. (f) Quantitative analysis of differentiation efficacy expressed as the number of TuJ-1 positive cells (*N*) over total cell population ($N_{tot}$) for C17.2 cells after 24 h of incubation. Data are expressed as mean ± SD for at least 500 cells per condition (*n* = 4). The degree of significance between treated samples and control samples are indicated when appropriate (**p* < 0.05; ***p* < 0.01; ****p* < 0.001). In a–f, solid lines correspond to C17.2 neural progenitor cells and dotted lines correspond to primary HUVEC cells. Squares correspond to positively charged NPs and circles to negatively charged NPs.**

location of the NPs. In particular, it is important to differentiate between the concentration of NPs that is externally applied and the concentration of the NPs within the cell. Our uptake data demonstrate that, at equivalent extracellular NP concentration, the concentration of internalized NPs is greater for positively than for negatively charged NPs. Although the precise nature of the cytotoxic effects observed in our study remains elusive, the data obtained here indicate that they are related to the intracellular NP level rather than to the concentration of NPs to which the cells were exposed, in agreement with earlier reports on various types of NPs.[23,53,54]

Taking together all our cytotoxicity data, the concentrations above which adverse effects are observable can be defined as 20 nM for the negatively charged NPs and 5 nM for the positively charged ones, indicating a clear effect of the NP surface charge on cytotoxicity, mainly driven by their higher cellular uptake.

## CONCLUSIONS

Our data indicate that positively charged NPs are incorporated faster than negatively charged NPs by several cell lines, while they also possess higher cytotoxic potential. Similar findings have been reported before, *i.e.*, there have been claims that higher cytotoxic potential of positively charged NPs is predominantly related with higher cellular uptake of these NPs. However, by using highly defined and well characterized

NPs, our study contributes further insights into the charge-dependent interaction of these NPs with cells. Our study points to the problem that several physicochemical parameters are entangled. Despite symmetric surface chemistry of our negatively and positively charged NPs, the negatively charged NPs used in this study had a lower colloidal stability than their positively charged counterparts. This may well affect cellular uptake, which is known to be size dependent. The key point of the present study is the use of NPs with good colloidal stability, thereby keeping the effective size (hydrodynamic diameter) constant and avoiding formation of large agglomerates, so that the effect of the net surface charge is decoupled from the effects NP size and agglomeration.

Parallel to the analysis of the colloidal stability and the formation of the protein corona, the uptake kinetics of the NPs by cells were recorded. Many studies report that uptake of NPs is mainly influenced by the protein corona. Protein adsorption relies on interaction with charged spots on the proteins.[25] If the charge on the NP is reverted, proteins may adsorb to the NPs such that the charge on the outside of the corona will be reverted. In our experiments, the qualitative formation of the protein corona (as determined from the amount of adsorbed HSA proteins upon exposure to HSA) was similar for negatively and positively charged NPs, though their uptake behavior by cells differed drastically. It has to be pointed out, however, that our FCS data are sensitive only to changes in the size of the adsorbed protein (HSA) corona, but do not give information about the internal structure of the proteins. In fact, with or without the presence of a protein corona, clear differences depending on the surface charge are visible. As differences in cellular uptake were also observed in media without proteins, we conclude that the sign of the charge (and eventually associated changes in colloidal stability) is also a direct parameter which determines quantitative uptake of NPs. Associated changes in the structure of the protein corona will play an additional role compared to the direct charge effect. There is also a clear correlation between uptake of NPs and their corresponding toxic effects on cells, which in both cases are higher for positively than for negatively charged NPs.

## MATERIALS AND METHODS

**NP Synthesis.** Colloidal Au NPs were synthesized in organic solvents according to standard procedures.[55] Transmission electron microscopy (TEM) analysis indicated an inorganic core diameter of $d_c$ = 4.6 ± 1.1 nm. To transfer the NPs into an aqueous solution, they were enshrouded by an amphiphilic polymer shell.[56] Negatively and positively charged co- and terpolymers of type poly((2-(methacryloyloxy)ethyl)phosphonic acid)$_x$-*stat*-poly(lauryl methacrylate)$_y$-*stat*-poly(propargyle methacrylate)$_z$ (PMAPHOS-*stat*-PLMA-*stat*-PgMA) and poly(*N*,*N*,*N*-trimethylamonium-2-ethyl methacrylate iodide)$_x$-*stat*-poly(lauryl methacrylate)$_y$-*stat*-poly(propargyle methacrylate)$_z$ (PTMAEMA-*stat*-PLMA-*stat*-PgMA) which contained charged monomers (phosphonate or trimethylammonium groups, respectively) and monomers with hydrophobic side chains ($-C_{12}H_{25}$) were synthesized similar to a previously described protocol,[16] *cf.* Figure 1 and Table 1. The ratios of charged (*x*) to hydrophobic (*y*) monomers and the molecular weights were *x*:*y* = 40:60 (*z* = 0) and $M_n$ = 9000 g/mol, and *x*:*y* = 53:47 (*z* = 0) and $M_n$ = 16 300 g/mol for the negatively and positively charged copolymers, respectively. Both polymers thus had comparable molecular weights and compositions. They were selected on the basis of a prior study in which optimal conditions for colloidal stability were determined.[16] For the terpolymers, an additional monomer with an alkyne residue (PgMA) was added. The ratios of charged (*x*), hydrophobic (*y*), and functional (*z*) units and the molecular weights were *x*:*y*:*z* = 52:42:6 and $M_n$ = 9500 g/mol, and *x*:*y*:*z* = 48:48:4 and $M_n$ = 17 800 g/mol for the negatively and positively charged terpolymers, respectively. Monomers were assembled statistically. The red azide-modified fluorophore perylene tetracarboxylic diimide (PDI-$N_3$) was attached to the monomers carrying the alkyne function *via* the azide group using click chemistry.[57] The quantitative conversion was verified by UV/vis and $^1$H NMR spectroscopy (see Supporting Information). The dye provided the fluorescence contrast employed for cellular uptake studies. Recent investigations using the same polymer-coating technique with a different fluorophore demonstrated that the hydrophobic fluorophores were located inside the polymer shell rather than pointing toward the solution.[58] Consequently, we expect that the fluorophore in the polymer shell has only minimal, if any, influence on the NP interaction with cells. Polymers were added to the hydrophobic Au NPs, the organic solvent (chloroform) was evaporated, and the NPs became water-soluble upon addition of alkaline sodium borate buffer (SBB, pH = 12) and 0.1 M NaCl solution (pH = 3.3, adjusted with HCl) for negatively and positively charged polymers, respectively, following standard procedures.[16,56] The NPs were extensively purified by size exclusion chromatography and/or gel electrophoresis (the latter worked only for negatively charged NPs), leading to pure NP suspensions.[16] The effective quantum yields ($\Phi_s$) of the negatively and positively charged NPs (with fluorophore in their polymer shell) in water were $\Phi_s(-) = 0.053 \pm 0.003$ and $\Phi_s(+) = 0.057 \pm 0.004$, respectively (see Supporting Information). These "effective" quantum yields (= number of emitted photons emitted by PDI per number of incident photons reaching the Au-PDI hybrid particle) are significantly smaller than the quantum yield of PDI in solution because a significant fraction of incident light is absorbed by the Au NPs and not by PDI. A detailed description and all raw data are given in the Supporting Information.

**Physicochemical Characterization.** Extinction spectra of negatively and positively charged NPs with and without fluorophore were measured in different media (#2 to #8). In each case, the pure medium served as a blank. After addition of NPs at a concentration of 5 nM, an extinction spectrum was taken at different time points within 1 h. The added volume of NP solution was 2 orders of magnitude lower compared to the present volume of medium to maintain the physical conditions of the medium. The maximum absorbance between 500 and 600 nm comprising the surface plasmon peak and the dye absorbance (in case a fluorophore was present) was plotted against the time after addition of the NP solution.

**Investigation of Protein Adsorption in Different Media.** FCS measurements were performed on a homemade confocal microscope with single-molecule sensitivity similar to those reported previously.[59,60] The setup is based on an inverted microscope frame (Axiovert 135 TV, Zeiss, Oberkochen, Germany) and equipped with a home-made acousto-optical beam splitter (AOBS). A 532-nm laser excitation (power 6 $\mu$W) was focused onto the sample by a water immersion objective

(UPLAPO 60x/1.2w, Olympus, Hamburg, Germany). The emitted light was collected by the same objective and focused onto a 50 $\mu$m-diameter pinhole, passed through a 532 nm notch filter and 50/50 beam splitter cube and was detected by two avalanche photo diodes (SPCM-AQR 14, Perkin-Elmer, Boston, MA). Cross-correlation functions from the two detector outputs were calculated by a digital correlator (ALV 5000/E, ALV, Langen, Germany). All measurements were performed at 23 °C. NP suspensions were diluted to 4 nM with PBS buffer; HSA was diluted to the desired concentrations with PBS (medium #2) at room temperature (23 °C) and mixed in equal volumes with the dilute NP solution. Samples were incubated for 10 min just prior to the measurements. The autocorrelation functions were fitted with a model function for free diffusion with a three-dimensional Gaussian volume to obtain diffusional correlation times,[61] which can be converted into diffusion coefficients. Rhodamine 6G was used as a reference sample (diffusion coefficient $D = 4.14 \pm 0.05$ cm$^2$/s)[62] to calculate the hydrodynamic radii of the Au NPs. Diffusion coefficients were converted into hydrodynamic radii by the Stokes–Einstein equation. The change in hydrodynamic radius by concentration dependent adsorption of proteins on surfaces was fitted with a simple binding model[24,42] using

$$r_h = r_h(0)\left(1 + \frac{V_{HSA}}{\frac{4}{3}\pi r_h(0)^3} N_{max} \frac{1}{1 + (K_d/c(HSA))^n}\right)^{1/3} \quad (1)$$

Here, $r_h$ and $r_h(0)$ are the hydrodynamic radii of the protein-coated and bare NPs, respectively, $V_{HSA}$ and $c$(HSA) represent the molecular volume and concentration of HSA, respectively. Protein binding to the Au NPs is governed by three parameters, the maximum number of proteins bound per NP, $N_{max}$, the `apparent' binding coefficient, $K_d$, and the Hill coefficient, $n$.[62]

**Charge-Dependent Uptake of Nanoparticles.** 3T3 cells were incubated with negatively and positively charged Au NPs (with PDI-$N_3$ in their polymer shell) in different media (#5, #7 and #8). The experiments were carried out in different culture media in micro-8-well plates at 5% $CO_2$ atmosphere and 37 °C. The samples were analyzed with an Axiovert 200 M widefield microscope (Zeiss, Germany) with attached incubator stage at different time points of incubation. The obtained images (dark field + red fluorescence of fluorophore in NP shell) were analyzed with ImageJ. The mean intensity of a number of regions of interest (ROIs) inside the cell body and cell membrane excluding the nucleus was determined for around 30 cells per specimen. In all experiments, the background intensity was subtracted, and data were corrected for intrinsic differences in the fluorescence emission of Au NPs (see Supporting Information).

**Charge-Dependent Cytotoxicity of Nanoparticles.** The cytotoxic effects of the nanoparticles was investigated on primary human umbilical vein endothelial cells (HUVECs) and murine neural progenitor cells (C17.2). Essentially, these experiments were performed in serum-containing media, similar to medium #8. Cell viability was measured in both cell types for a range of nanoparticles concentrations (1–50 nM) after 24 h by an Alamar Blue assay (Molecular Probes, Invitrogen, Merelbeke, Belgium) according to the manufacturer's protocol. For the same concentration range, cell viability was qualitatively examined by means of Calcein AM/Ethidium homodimer co-incubation as described previously.[63] Oxidative stress was evaluated by means of the 5-(and-6)-chloromethyl-2′,7′-dichlorodihydrofluorescein diacetate, acetyl ester (CM-$H_2$DCFDA; Molecular Probes, Invitrogen, Merelbeke, Belgium) assay as described previously.[8] The effects of the nanoparticles on HUVEC morphology and C17.2 cell functionality were assessed as described elsewhere.[6,53] A detailed description can also be found in the Supporting Information.

*Conflict of Interest:* The authors declare no competing financial interest.

*Acknowledgment.* S.J.H.S. is a postdoctoral fellow from FWO-Vlaanderen. Financial support from FWO-Vlaanderen (Krediet aan Navorsers to S.J.H.S.), the Centre for Nano- and Biophotonics (Ghent University), and the Deutsche Forschungsgemeinschaft (DFG, SPP1313 and CFN) are gratefully acknowledged.

*Supporting Information Available:* Full methodology and additional data are available free of charge *via* the Internet at http://pubs.acs.org.

## REFERENCES AND NOTES

1. Rivera_Gil, P.; Jimenez de Aberasturi, D.; Wulf, V.; Pelaz, B.; del Pino, P.; Zhao, Y.; de la Fuente, J.; Ruiz de Larramendi, I.; Rojo, T.; Liang, X.-J.; et al. The Challenge to Relate the Physicochemical Properties of Colloidal Nanoparticles to Their Cytotoxicity. *Acc. Chem. Res.* **2013**, *46*, 743–749.
2. Rivera_Gil, P.; Oberdorster, G.; Elder, A.; Puntes, V. F.; Parak, W. J. Correlating Physico-Chemical with Toxicological Properties of Nanoparticles: The Present and the Future. *ACS Nano* **2010**, *4*, 5527–5531.
3. Tanguay, R. L.; Harper, S. L.; Carriere, J. L.; Miller, J. M.; Hutchison, J. E.; Maddux, B. L. S. Systematic Evaluation of Nanomaterial Toxicity: Utility of Standardized Materials and Rapid Assays. *ACS Nano* **2011**, *5*, 4688–4697.
4. Asati, A.; Santra, S.; Kaittanis, C.; Perez, J. M. Surface-Charge-Dependent Cell Localization and Cytotoxicity of Cerium Oxide Nanoparticles. *ACS Nano* **2010**, *4*, 5321–5331.
5. Verma, A.; Stellacci, F. Effect of Surface Properties on Nanoparticle-Cell Interactions. *Small* **2010**, *6*, 12–21.
6. Soenen, S. J. H.; Himmelreich, U.; Nuytten, N.; De Cuyper, M. Cytotoxic Effects of Iron Oxide Nanoparticles and Implications for Safety in Cell Labelling. *Biomaterials* **2011**, *32*, 195–205.
7. Schweiger, C.; Hartmann, R.; Zhang, F.; Parak, W. J.; Kissel, T.; Rivera_Gil, P. Quantification of the Internalization Patterns of Superparamagnetic Iron Oxide Nanoparticles with Opposite Charge. *J. Nanobiotechnol.* **2012**, *10*, 28.
8. Soenen, S. J. H.; Demeester, J.; De Smedt, S. C.; Braeckmans, K. The Cytotoxic Effects of Polymer-Coated Quantum Dots and Restrictions for Live Cell Applications. *Biomaterials* **2012**, *33*, 4882–4888.
9. Ojea-Jiménez, I.; García-Fernández, L.; Lorenzo, J.; Puntes, V. F. Facile Preparation of Cationic Gold Nanoparticle-Bioconjugates for Cell Penetration and Nuclear Targeting. *ACS Nano* **2012**, *6*, 7692–7702.
10. Goodman, C. M.; McCusker, C. D.; Yilmaz, T.; Rotello, V. M. Toxicity of Gold Nanoparticles Functionalized with Cationic and Anionic Side Chains. *Bioconjugate Chem.* **2004**, *15*, 897–900.
11. Hirsch, V.; Kinnear, C.; Moniatte, M.; Rothen-Rutishauser, B.; Clift, M. J. D.; Fink, A. Surface Charge of Polymer Coated SPIONs Influences the Serum Protein Adsorption, Colloidal Stability and Subsequent Cell Interaction in Vitro. *Nanoscale* **2013**, 10.1039/C2NR33134A.
12. Tycko, B.; Maxfield, F. R. Rapid Acidification of Endocytic Vesicles Containing Alpha-2-Macroglobulin. *Cell* **1982**, *28*, 643–651.
13. Yu, W. W.; Chang, E.; Falkner, J. C.; Zhang, J. Y.; Al-Somali, A. M.; Sayes, C. M.; Johns, J.; Drezek, R.; Colvin, V. L. Forming Biocompatible and Nonaggregated Nanocrystals in Water Using Amphiphilic Polymers. *J. Am. Chem. Soc.* **2007**, *129*, 2871–2879.
14. Yu, W. W.; Chang, E.; Sayes, C. M.; Drezek, R.; Colvin, V. L. Aqueous Dispersion of Monodisperse Magnetic Iron Oxide Nanocrystals through Phase Transfer. *Nanotechnology* **2006**, *17*, 4483–4487.
15. Chanana, M.; Rivera_Gil, P.; Correa-Duarte, M. A.; Liz-Marzán, L. M.; Parak, W. J. Physicochemical Properties of Protein-Coated Gold Nanoparticles in Biological Fluids and Cells Before and After Proteolytic Digestion. *Angew. Chem., Int. Ed. Engl.* **2013**, DOI: 10.1002/anie.201208019.s.
16. Geidel, C.; Schmachtel, S.; Riedinger, A.; Pfeiffer, C.; Müllen, K.; Klapper, M.; Parak, W. J. A General Synthetic Approach for Obtaining Cationic and Anionic Inorganic Nanoparticles *via* Encapsulation in Amphiphilic Copolymers. *Small* **2011**, *7*, 2929–2934.
17. Brown, W.; Zhao, J. X. Adsorption of Sodium Dodecyl-Sulfate on Polystyrene Latex-Particles Using Dynamic

Light-scattering and Zeta-Potential Measurements. *Macromolecules* **1993**, *26*, 2711–2715.
18. Loeb, J. The Influence of Electrolytes on the Cataphoretic Charge of Colloidal Particles and the Stability of their Suspensions. I. Experiments with Collodion Particles. *J. Gen. Physiol.* **1922**, *5*, 109–126.
19. Puertas, A. M.; de las Nieves, F. J. Colloidal Stability of Polymer Colloids with Variable Surface Charge. *J. Colloid Interface Sci.* **1999**, *216*, 221–229.
20. Casals, E.; Pfaller, T.; Duschl, A.; Oostingh, G. J.; Puntes, V. F. Time Evolution of the Nanoparticle Protein Corona. *ACS Nano* **2010**, *4*, 3623–3632.
21. Cedervall, T.; Lynch, I.; Lindman, S.; Berggård, T.; Thulin, E.; Nilsson, H.; Dawson, K. A.; Linse, S. Understanding the Nanoparticle-Protein Corona Using Methods to Quantify Exchange Rates and Affinities of Proteins for Nanoparticles. *Proc. Natl. Acad. Sci. U.S.A.* **2007**, *104*, 2050–2055.
22. Lundqvist, M.; Stigler, J.; Elia, G.; Lynch, I.; Cedervall, T.; Dawson, K. A. Nanoparticle Size and Surface Properties Determine the Protein Corona with Possible Implications for Biological Impacts. *Proc. Natl. Acad. Sci. U.S.A.* **2008**, *105*, 14265–14270.
23. Maiorano, G.; Sabella, S.; Sorce, B.; Brunetti, V.; Malvindi, M. A.; Cingolani, R.; Pompa, P. P. Effects of Cell Culture Media on the Dynamic Formation of Protein-Nanoparticle Complexes and Influence on the Cellular Response. *ACS Nano* **2010**, *4*, 7481–7491.
24. Röcker, C.; Pötzl, M.; Zhang, F.; Parak, W. J.; Nienhaus, G. U. A Quantitative Fluorescence Study of Protein Monolayer Formation on Colloidal Nanoparticles. *Nat. Nanotechnol.* **2009**, *4*, 577–580.
25. Maffre, P.; Nienhaus, K.; Amin, F.; Parak, W. J.; Nienhaus, G. U. Characterization of Protein Adsorption onto FePt Nanoparticles Using Dual-Focus Fluorescence Correlation Spectroscopy. *Beilstein J. Nanotechnol.* **2011**, *2*, 374–383.
26. Tenzer, S.; Docter, D.; Rosfa, S.; Wlodarski, A.; Kuharev, J.; Rekik, A.; Knauer, S. K.; Bantz, C.; Nawroth, T.; Bier, C.; et al. Nanoparticle Size is a Critical Physicochemical Determinant of the Human Blood Plasma Corona: A Comprehensive Quantitative Proteomic Analysis. *ACS Nano* **2011**, *5*, 7155–67.
27. Monopoli, M. P.; Aberg, C.; Salvati, A.; Dawson, K. A. Biomolecular Coronas Provide the Biological Identity of Nanosized Materials. *Nat. Nanotechnol.* **2012**, *7*, 779–786.
28. Lesniak, A.; Campbell, A.; Monopoli, M. P.; Lynch, I.; Salvati, A.; Dawson, K. A. Serum Heat Inactivation Affects Protein Corona Composition and Nanoparticle Uptake. *Biomaterials* **2010**, *31*, 9511–9518.
29. Harford, C. G.; Hamlin, A.; Parker, E. Electron Microscopy of HeLa Cells after the Ingestion of Colloidal Gold. *J. Biophys. Biochem. Cytol.* **1957**, *3*, 749–756.
30. Muller-Borer, B. J.; Collins, M. C.; Gunst, P. R.; Cascio, W. E.; Kypson, A. P. Quantum Dot Labeling of Mesenchymal Stem Cells. *J. Nanobiotechnol.* **2007**, *5*, 1–9.
31. Derfus, A. M.; Chan, W. C. W.; Bhatia, S. N. Intracellular Delivery of Quantum Dots for Live Cell Labeling and Organelle Tracking. *Adv. Mater. (Weinheim, Ger.)* **2004**, *16*, 961–966.
32. Brandenberger, C.; Mühlfeld, C.; Ali, Z.; Lenz, A.-G.; Schmid, O.; Parak, W. J.; Gehr, P.; Rothen-Rutishauser, B. Quantitative Evaluation of Cellular Uptake and Trafficking of Plain and Polyethylene Glycol-Coated Gold Nanoparticles. *Small* **2010**, *6*, 1669–1678.
33. Jiang, X.; Röcker, C.; Hafner, M.; Nienhaus, G. U. Endo- and Exocytosis of Zwitterionic Quantum Dot Nanoparticles by Living Cells. *ACS Nano* **2010**, *4*, 6787–6797.
34. Harush-Frenkel, O.; Rozentur, E.; Benita, S.; Altschuler, Y. Surface Charge of Nanoparticles Determines their Endocytic and Transcytotic Pathway in Polarized MDCK Cells. *Biomacromolecules* **2008**, *9*, 435–443.
35. Jung, T.; Kamm, W.; Breitenbach, A.; Kaiserling, E.; Xiao, J. X.; Kissel, T. Biodegradable Nanoparticles for Oral Delivery of Peptides: Is there a Role for Polymers to Affect Mucosal Uptake? *Eur. J. Pharm. Biopharm.* **2000**, *50*, 147–160.
36. Rabinovich-Guilatt, L.; Couvreur, P.; Lambert, G.; Dubernet, C. Cationic Vectors in Ocular Drug Delivery. *J. Drug Targeting* **2004**, *12*, 623–633.
37. Bartneck, M.; Keul, H. A.; Wambach, M.; Bornemann, J.; Gbureck, U.; Chatain, N.; Neuss, S.; Tacke, F.; Groll, J.; Zwadlo-Klarwasser, G. Effects of Nanoparticle Surface Coupled Peptides, Functional Endgroups, and Charge on Intracellular Distribution and Functionality of Human Primary Reticuloendothelial Cells. *Nanomedicine (New York, NY, U.S.)* **2012**, *8*, 1282–1292.
38. Bhattacharjee, S.; Ershov, D.; van der Gucht, J.; Alink, G. M.; Rietjens, I. M. C. M.; Zuilhof, H.; Marcelis, A. T. M. Surface Charge-Specific Cytotoxicity and Cellular Uptake of Tri-Block Copolymer Nanoparticles. *Nanotoxicology* **2013**, *7*, 71–84.
39. Jiang, X.; Musyanovych, A.; Röcker, C.; Landfester, K.; Mailander, V.; Nienhaus, G. U. Specific Effects of Surface Carboxyl Groups on Anionic Polystyrene Particles in their Interactions with Mesenchymal Stem Cells. *Nanoscale* **2011**, *3*, 2028–2035.
40. Jiang, X.; Dausend, J.; Hafner, M.; Musyanovych, A.; Röcker, C.; Landfester, K.; Mailander, V.; Nienhaus, G. U. Specific Effects of Surface Amines on Polystyrene Nanoparticles in their Interactions with Mesenchymal Stem Cells. *Biomacromolecules* **2010**, *11*, 748–753.
41. Muñoz Javier, A.; Kreft, O.; Piera Alberola, A.; Kirchner, C.; Zebli, B.; Susha, A. S.; Horn, E.; Kempter, S.; Skirtach, A. G.; Rogach, A. L.; et al. Combined Atomic Force Microscopy and Optical Microscopy Measurements as a Method to Investigate Particle Uptake by Cells. *Small* **2006**, *2*, 394–400.
42. Jiang, X.; Weise, S.; Hafner, M.; Röcker, C.; Zhang, F.; Parak, W. J.; Nienhaus, G. U. Quantitative Analysis of the Protein Corona on FePt Nanoparticles Formed by Transferrin Binding. *J. R. Soc., Interface* **2010**, *7*, S5–S13.
43. Lesniak, A.; Fenaroli, F.; Monopoli, M. R.; Aberg, C.; Dawson, K. A.; Salvati, A. Effects of the Presence or Absence of a Protein Corona on Silica Nanoparticle Uptake and Impact on Cells. *ACS Nano* **2012**, *6*, 5845–5857.
44. Semmling, M.; Kreft, O.; Muñoz Javier, A.; Sukhorukov, G. B.; Käs, J.; Parak, W. J. A Novel Flow-Cytometry-based Assay for Cellular Uptake Studies of Polyelectrolyte Microcapsules. *Small* **2008**, *4*, 1763–1768.
45. Soenen, S. J. H.; Brisson, A. R.; Jonckheere, E.; Nuytten, N.; Tan, S.; Himmelreich, U.; De Cuyper, M. The Labeling of Cationic Iron Oxide Nanoparticle-Resistant Hepatocellular Carcinoma Cells Using Targeted Magnetoliposomes. *Biomaterials* **2011**, *32*, 1748–1758.
46. Bexiga, M. G.; Varela, J. A.; Wang, F. J.; Fenaroli, F.; Salvati, A.; Lynch, I.; Simpson, J. C.; Dawson, K. A. Cationic Nanoparticles Induce Caspase 3-, 7- and 9-Mediated Cytotoxicity in a Human Astrocytoma Cell Line. *Nanotoxicology* **2011**, *5*, 557–567.
47. Soenen, S. J. H.; Rivera_Gil, P.; Montenegro, J. M.; Parak, W. J.; De Smedt, S. C.; Braeckmans, K. Cellular Toxicity of Inorganic Nanoparticles: Common Aspects and Guidelines for Improved Nanotoxicity Evaluation. *Nano Today* **2011**, *6*, 446–465.
48. Nel, A. E.; Madler, L.; Velegol, D.; Xia, T.; Hoek, E. M. V.; Somasundaran, P.; Klaessig, F.; Castranova, V.; Thompson, M. Understanding Biophysicochemical Interactions at the Nano-Bio Interface. *Nat. Mater.* **2009**, *8*, 543–557.
49. Pan, Y.; Leifert, A.; Ruau, D.; Neuss, S.; Bornemann, J.; Schmid, G.; Brandau, W.; Simon, U.; Jahnen-Dechent, W. Gold Nanoparticles of Diameter 1.4 nm Trigger Necrosis by Oxidative Stress and Mitochondrial Damage. *Small* **2009**, *5*, 2067–2076.
50. Mironava, T.; Hadjiargyrou, M.; Simon, M.; Jurukovski, V.; Rafailovich, M. H. Gold Nanoparticles Cellular Toxicity and Recovery: Effect of Size, Concentration and Exposure Time. *Nanotoxicology* **2010**, *4*, 120–137.
51. Pernodet, N.; Fang, X. H.; Sun, Y.; Bakhtina, A.; Ramakrishnan, A.; Sokolov, J.; Ulman, A.; Rafailovich, M. Adverse Effects of Citrate/Gold Nanoparticles on Human Dermal Fibroblasts. *Small* **2006**, *2*, 766–773.
52. Shapero, K.; Fenaroli, F.; Lynch, I.; Cottell, D. C.; Salvati, A.; Dawson, K. A. Time and Space Resolved Uptake Study of Silica Nanoparticles by Human Cells. *Mol. BioSyst.* **2011**, *7*, 371–378.

53. Soenen, S. J. H.; Nuytten, N.; De Meyer, S. F.; De Smedt, S. C.; De Cuyper, M. High Intracellular Iron Oxide Nanoparticle Concentrations Affect Cellular Cytoskeleton and Focal Adhesion Kinase-Mediated Signaling. *Small* **2010**, *6*, 832–842.
54. Soenen, S. J. H.; De Meyer, S. F.; Dresselaers, T.; Velde, G. V.; Pareyn, I. M.; Braeckmans, K.; De Cuyper, M.; Himmelreich, U.; Vanhoorelbeke, K. I. MRI Assessment of Blood Outgrowth Endothelial Cell Homing Using Cationic Magnetoliposomes. *Biomaterials* **2011**, *32*, 4140–4150.
55. Brust, M.; Walker, M.; Bethell, D.; Schiffrin, D. J.; Whyman, R. Synthesis of Thiol-Derivatized Gold Nanoparticles in a 2-Phase Liquid-Liquid System. *J. Chem. Soc., Chem. Commun.* **1994**, 801–802.
56. Lin, C.-A. J.; Sperling, R. A.; Li, J. K.; Yang, T.-Y.; Li, P.-Y.; Zanella, M.; Chang, W. H.; Parak, W. J. Design of an Amphiphilic Polymer for Nanoparticle Coating and Functionalization. *Small* **2008**, *4*, 334–341.
57. Kolb, H. C.; Finn, M. G.; Sharpless, K. B. Click Chemistry: Diverse Chemical Function from a Few Good Reactions. *Angew. Chem., Int. Ed.* **2001**, *40*, 2004–2021.
58. Amin, F.; Yushchenko, D. A.; Montenegro, J. M.; Parak, W. J. Integration of Organic Fluorophores in the Surface of Polymer-Coated Colloidal Nanoparticles for Sensing the Local Polarity of the Environment. *ChemPhysChem* **2012**, *13*, 1030–1035.
59. Schenk, A.; Ivanchenko, S.; Röcker, C.; Wiedenmann, J. R.; Nienhaus, G. U. Photodynamics of Red Fluorescent Proteins Studied by Fluorescence Correlation Spectroscopy. *Biophys. J.* **2004**, *86*, 384–394.
60. Kobitski, A. Y.; Nierth, A.; Helm, M.; Jaschke, A.; Nienhaus, G. U. $Mg^{2+}$-Dependent Folding of a Diels-Alderase Ribozyme Probed by Single-Molecule FRET Analysis. *Nucleic Acids Res.* **2007**, *35*, 2047–2059.
61. Elson, E. L.; Magde, D. Fluorescence Correlation Spectroscopy. 1. Conceptual Basis and Theory. *Biopolymers* **1974**, *13*, 1–27.
62. Müller, C. B.; Loman, A.; Pacheco, V.; Koberling, F.; Willbold, D.; Richtering, W.; Enderlein, J. Precise Measurement of Diffusion by Multi-Color Dual-Focus Fluorescence Correlation Spectroscopy. *Europhys. Lett.* **2008**, *83*, 46001.
63. Soenen, S. J. H.; De Cuyper, M. How to Assess Cytotoxicity of (Iron Oxide-Based) Nanoparticles. A Technical Note Using Cationic Magnetoliposomes. *Contrast Media Mol. Imaging* **2011**, *6*, 153–164.